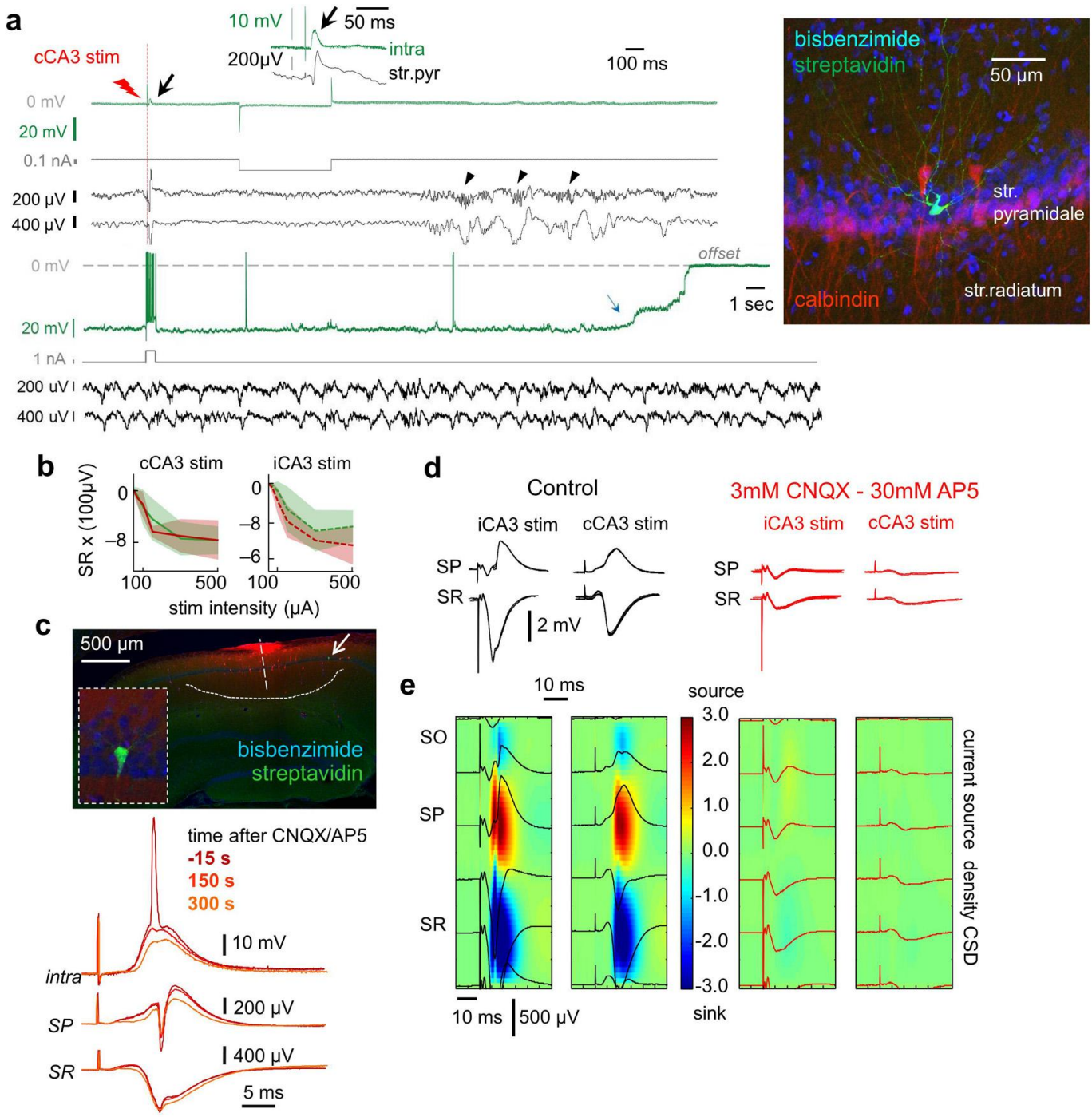

Supplementary Figure 1

Methodological approaches and pharmacological manipulations in vivo

(**a**) Steps in the process of intracellular impalement of pyramidal cells in the dorsal hippocampus of Wistar rats under urethane (1.2 g/kg). Top traces; before entering the cell, we confirmed similar extracellular deflections in the sharp pipette (green) as compared to the silicon-probe site at the str.pyramidale (black traces; inset). Upper LFP traces: st.pyramidale, bottom trace str.radiatum. Note SPW-ripples indicated by arrowheads. Negative current injections were used to monitor input resistance. Bottom traces, after completing recording and labeling with positive current pulses, the electrode was retracted while monitoring cell survival. Once out the cell, the offset was estimated and corrected if required. Right, identification of the previous cell (visualized with streptavidin, green) as a deep

calbindin (red) immunonegative CA1 pyramidal cell. Bisbenzimide (blue) is used to identify cell nuclei. (**b**) Stimulation to the contralateral (cCA3) and ipsilateral (iCA3) CA3 region of the dorsal hippocampus was applied in a range from 50 to 500 µA. Note similar input/output responses recorded at the str.radiatum for depolarized (green; n=11 for cCA3, n=4 for iCA3) and hyperpolarized cells (red; n=7 for cCA3, n=4 for iCA3) discarding any potential influence of different stimulation intensities between groups. cCA3: p=0.839, F(2.12,14.85)=0.192; iCA3: p=0.471, F(1.10; 4.37)=0.729; repeated measures ANOVA. (**c**) Pharmacological interventions in vivo. Top, epifluorescence image of one representative experiment (of n=2 rats) showing the estimated extent of drug infusion (dotted curve) into the dorsal hippocampus as marked by the low molecular weight dextran Texas Red. For these experiments a silica tube (90 µm) glued to a 16 channel silicon probe (only last 8 channels at the tip were functional) was used for local delivery (Neuronexus D-series). Probe track is marked by a discontinuous line. Arrow points to the recorded cell, which is shown at the inset at higher magnification (confocal image taken at 40x, average intensity projection of z-stack, 24 µm). Bottom, evolution of the intracellular and extracellular CA3-evoked responses to contralateral stimulation before and after infusion of 3 mM CNQX and 30 mM AP5 (in ACSF containing in mM: 124 NaCl, 5 KCl, 1.5 $MgSO_4$, 26 $NaHCO_3$, 10 Glucose, pH 7.3, then bubbled with 95% O_2-5% CO_2, and 3mM $CaCl_2$) to block fast glutamatergic transmission. Note response decrease over time. Cell recording was lost after 5 minutes delivery preventing us to continue monitoring intracellular responses. (**d**) Extracellular LFP evoked responses at the str.pyramidale (SP) and radiatum (SR) were monitored over the entire course of the experiment for both the ipsilateral (iCA3) and contralateral (cCA3) stimulation. Same experiment as shown in **c**. Note the typical phase reversal of LFP signals between SP and SR before delivery (control), and the propagated shape of these signals 10 min after local delivery of CNQX/AP5. (**e**) Current source density (CSD) analysis confirmed full blockade of all CA3-evoked active currents, including any potentially direct GABAergic stimulation (confirmed for low and high stimulation intensities). These experiments support the interpretation of evoked GABAergic responses elicited in CA1 pyramidal cells by feedforward inhibition.

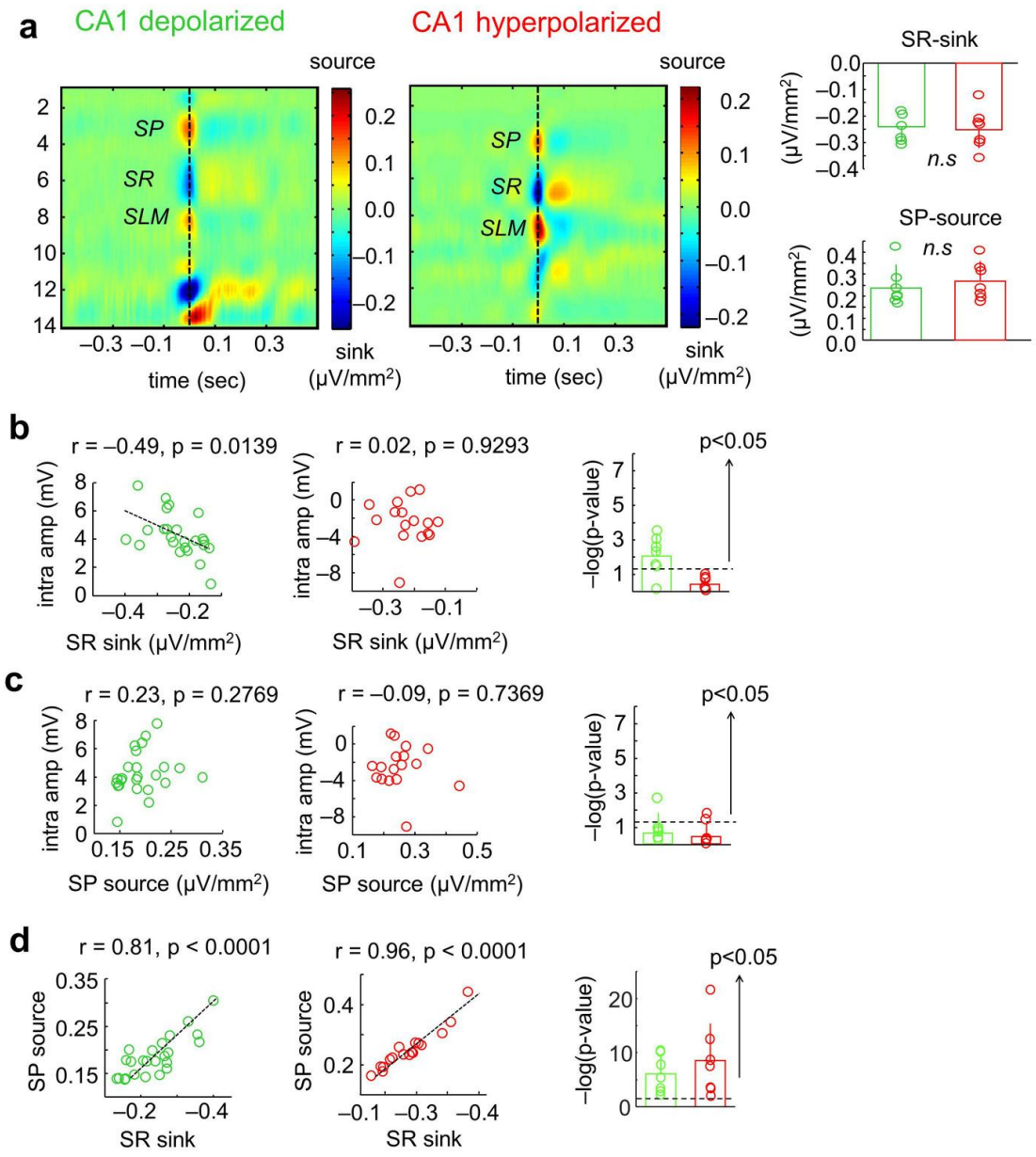

Supplementary Figure 2

Relationship between SPW sinks and sources and the intracellular membrane potential

(**a**) To examine co-variations between the SPW-ripple associated intracellular responses and the associated sink and sources, CSD signals were estimated from LFP recordings. Examples of mean CSD signals obtained from all events included in the analysis (aligned at the SPW peak, discontinuous vertical line) of one representative depolarized (green, left) and one representative hyperpolarized (red, right) cell. SPW-ripples were typically associated with a dominant sink (blue) at the str.radiatum (SR) in association with a CSD source at the str.pyramidale (SP). (Ylinen et al. 1995). Only cells with more than 10 intracellular sweeps at resting membrane potentials between -60 mV and -50 mV were included in the analysis (n=7 depolarized, n=7 hyperpolarized). Right, no differences for the amplitude of the SR sink and the SP source accounted for differences between cell groups. (**b**) Covariation between the SPW-

associated intracellular response measured at the SPW-ripple peak at resting membrane potential as a function of the amplitude of SR sink reveal strong correlation of depolarized responses (green) but poor correlation of hyperpolarized responses (red). Data from two representative cells from each group are shown. Each dot represents data from one event in a given cell. Rightmost, plot of the –log10(p-value) of the linear fit for each cell confirms most depolarized cells (6/7) exhibited significant correlation between the intracellular depolarization and the amplitude of the SR sink. Discontinuous line marks the statistical limit -log10(0.05)=1.3. No hyperpolarized cells (0/7) showed significant correlation. (**c**) Same analysis as in **a** (same cells) for the SP source. Rightmost, plot of the –log10(p-value) of the linear fit suggest poor intracellular correlation with the SP source. Only 1/7 depolarized and 2/7 hyperpolarized cells showed significant correlation. (**d**) Significant relationship between the SR sink and the SR source for the events used in **b** and **c** confirms specificity of intra-sink interactions. Rightmost, p-values from all cells examined are significant.

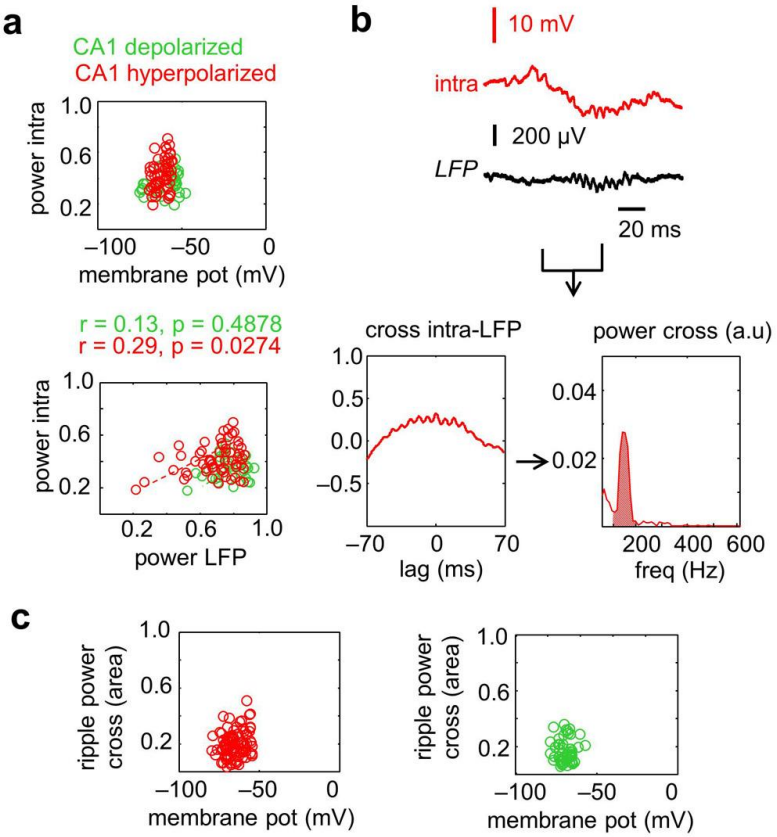

Supplementary Figure 3

Analysis of intracellular and extracellular ripple oscillations

(**a**) Dependence between the spectral power (area within 90-200 Hz) of SPW-associated intracellular ripple oscillations and the holding membrane potential in a representative hyperpolarized (red) and depolarized cell (green). Note poor correlation with membrane potential, but large event-to-event variability at a given holding potential, reflecting that dynamic fluctuations of individual SPW-ripples dominate. A mean value of the intracellular ripple power was estimated from all events detected in a given cell (range 10-112; 37 ± 27 events). Bottom, relationship between the power of the intracellular and extracellular ripple. Significant correlation was detected in some hyperpolarized cells. (**b**) To quantify intracellular-extracellular ripple coordination we estimated the cross-correlation function between individual sweeps and calculated the power spectrum of the cross-correlation. Bottom, a measure of intracellular-extracellular ripple coordination was defined from the spectral area in the 100-200 Hz band. (**c**) Dependence between the intracellular-extracellular ripple coordination and membrane potential. No correlation was evident from the entire dataset for any cell group.

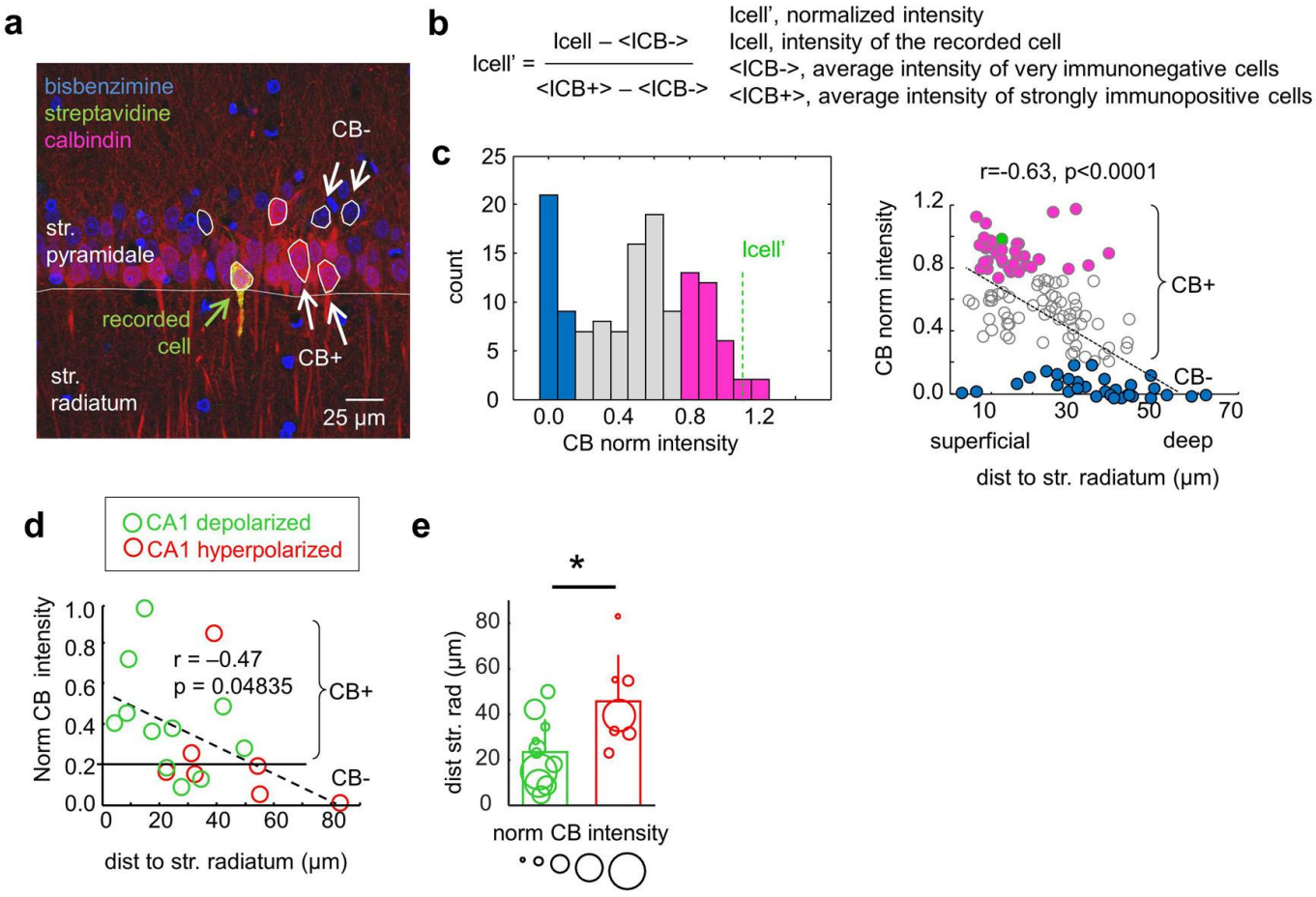

Supplementary Figure 4

Measurement of calbindin immunoreactivity on intracellular recorded cells

(**a**) Intensity of calbindin immunoreactivity was measured in recorded (n=18) and neighboring dorsal CA1 pyramidal cells (PCs) from single optical sections (0.97-1.88 µm thickness, 20x or 40x magnification). Regions of interest (ROIs) were drawn for 4-5 cells lacking detectable immunoreactivity (CB-, blue) and 4-5 cells with the apparent highest intensity (CB+, magenta), together with the recorded cell (green, cell I030414D8C2). ROIs drawn at 20x or 40x for the same cells gave similar results. Sparse intensely CB+ interneurons were not included, but some of the sampled CB- cells may be interneurons. (**b**) Mean gray values were obtained from these ROIs and normalized according to a formula, giving values between 0 (CB-) and 1 (maximal intensity of calbindin immunoreactivity, CB+). The normalized intensity of the recorded cell was calculated for subsequent classification and analysis. (**c**) An example histogram distribution (from n=8) for all cells in a representative image (20x, one optical section, 1.7 µm, 129 cells) reflects different levels of calbindin immunoreactivity with a high proportion of cells showing low-intermediate values. The recorded cell was classified as CB+. Right, the normalized intensity level (same data as in **c**) correlates with the distance to radiatum, with strongest calbindin immunoreactivity detected in somata near to the border (superficial cells), and no calbindin immunoreactivity in cells located far away from this border (deep cells) (n=129 cells, $p<0.0001$, $r(127)=-0.6251$; Pearson correlation). A binary classification of CB+ and CB- pyramidal cells was adopted, with clearly immunonegative cells being classified as CB- (intensity <0.2; blue) and neurons showing intense (intensity >0.75; magenta) and intermediate immunoreactivity to calbindin all being grouped as CB+. The recorded cell (green) can be thus classified as CB+. (**d**) Relationship between normalized calbindin intensity and the distance to radiatum in recorded cells. Note depolarized cells tend to be superficial (green, n=11) whereas hyperpolarized cells tend to be deep (n=7). A majority of hyperpolarized cells were immunonegative to calbindin (5/7). Most depolarized cells exhibited some level of calbindin immunoreactivity (8/11). Note however some variability in calbindin immunoreactivity and the electrophysiological identity (**e**) Significant group differences in the distance to radiatum is represented together with information from calbindin immunoreactivity (dot size)

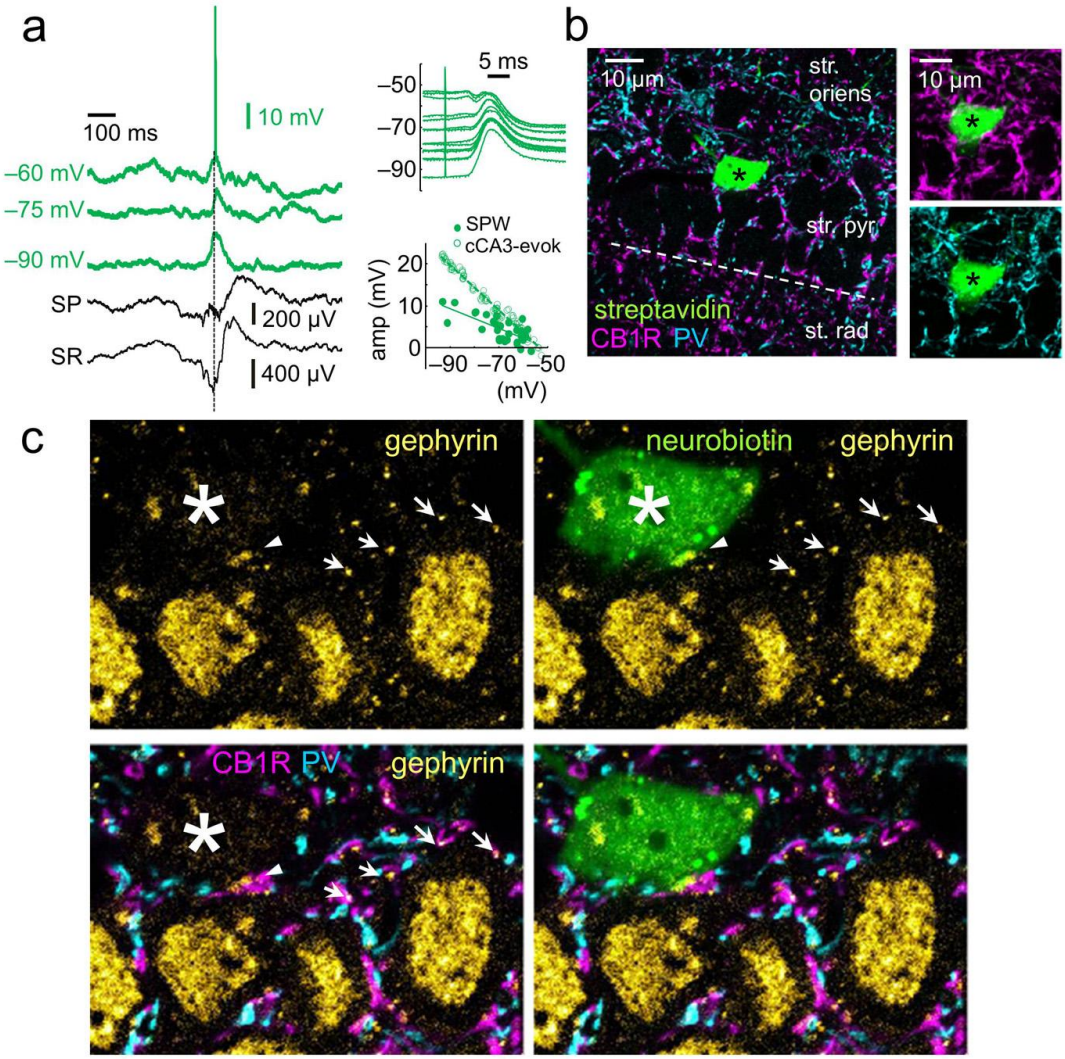

Supplementary Figure 5

Lack of gephyrin immunoreactivity in recorded pyramidal neurons.

(**a**) Intracellular activity of a CA1 pyramidal cell recorded in the urethane anesthetized preparation. This cell exhibited dominant depolarization during SPW-ripple events. Upper right, extracellular stimulation of the contralateral hippocampus allowed examination of the evoked responses. Lower right, note similar reversal potential of the SPW-associated and the contralateral CA3-evoked responses. Note reversal at about -50 mV in this cell. (**b**) Single optical section (0.29 µm thick) showing the neurobiotin-filled soma of the cell shown in **a** (green, asterisk) in the str.pyramidale amongst PV (magenta) and CB1R (cyan) immunoreactive processes. Dotted line, estimated border of strata radiatum and pyramidale. Right, average intensity projection (6.6 µm thick) of the soma (asterisk) surrounded by PV and CB1R immunoreactive terminals. (**c**), Single optical section (0.29 µm thick) of the recorded cell (green, asterisk) and adjacent unlabeled neurons. Four gephyrin puncta (arrows) within an unlabeled neuron are colocalized with presynaptic CB1R immunoreactive terminals (magenta). The recorded cell lacks gephyrin puncta for corresponding CB1R terminals. Non-specific labeling is observed (see nuclei and arrowheads).

a

	resting membrane potential (mV)	Tau (ms)	Rm (Momh)	Cm (pF)	n
Superficial	–57.8 ± 3.9	19.48 ± 5.4	115.0 ± 32.5	174.0 ± 39.2	21
Deep	–60.9 ± 3.3	20.13 ± 4.5	121.9 ± 20.5	164.7 ± 24.1	17
P-value	0.0135	0.694	0.449	0.398	

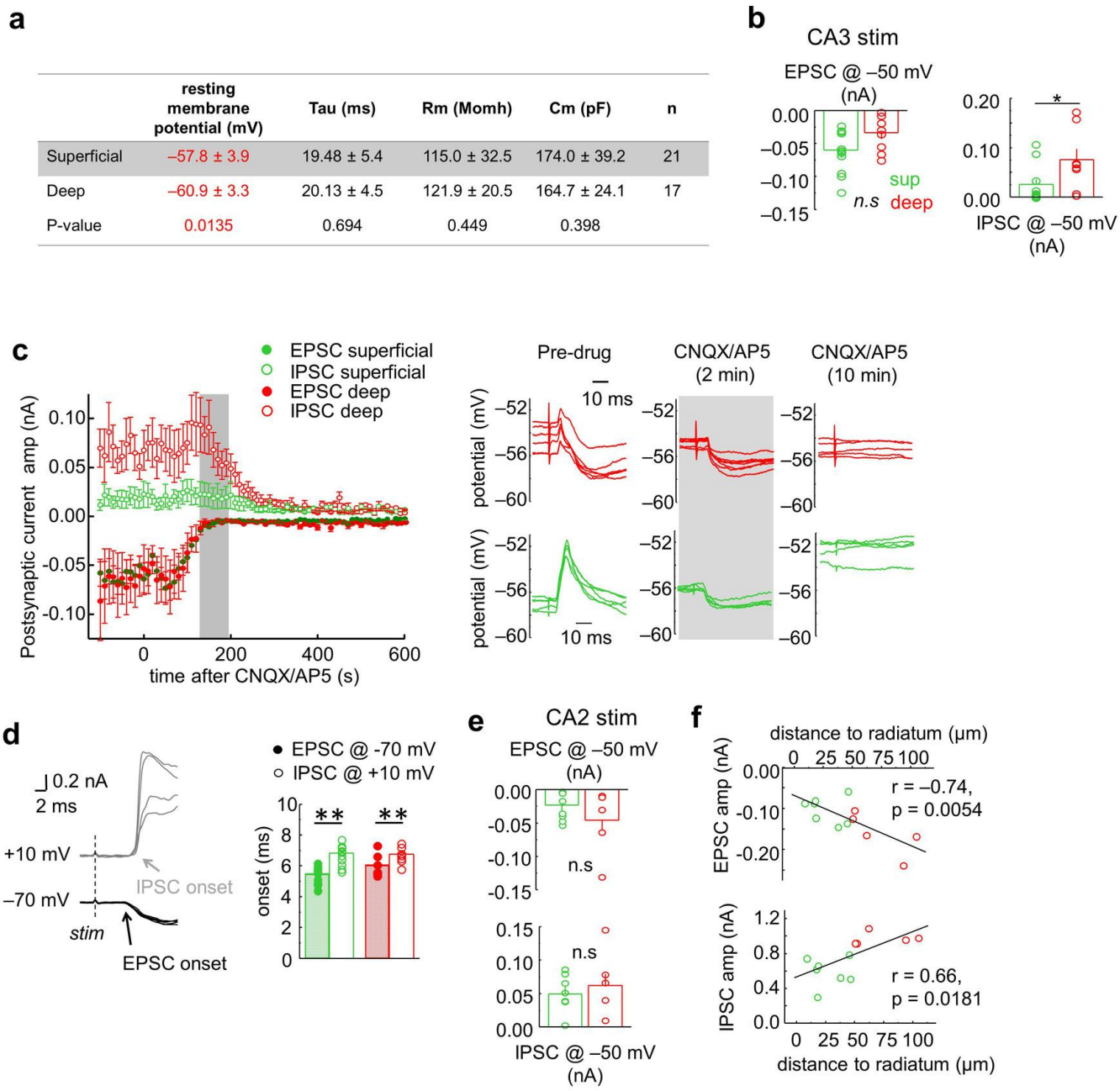

Supplementary Figure 6

In vitro analysis of synaptic currents in deep and superficial CA1 pyramidal cells

(**a**) Basic electrophysiological membrane properties of deep and superficial cells. Note significant differences in resting membrane potential. Estimation of the membrane time constant, input resistance and membrane capacitance was obtained at -60 mV. Data from all cells recorded in vitro. (**b**) Mean excitatory (EPSC) and inhibitory (IPSC) postsynaptic currents evoked in deep and superficial cells at -50 mV in response to CA3c stimulation. Data show significantly higher IPSCs at deep versus superficial cells (p=0.0471). While there was a non-significant trend of smaller EPSCs at – 50 mV in deep versus superficial cells (p=0.0671), this was not confirmed by EPSCs recorded at the GABAa-reversal potential at -70 mV (Fig.3E) suggesting potential contamination by outward IPSC currents. (**c**) Evolution of CA3-evoked EPSCs and IPSCs recorded at -50 mV before and after superfusion with 20 mM CNQX and 50 µM AP5. Data from n=6 deep, n=6 superficial cells. Note that after about 2 min superfusion of CNQX/AP5 glutamatergic EPSCs are blocked but

IPSCs currents can still be recorded (gray shadowed region) and confirmed stronger inhibition of deep cells. Full blockage of CA3-evoked IPSCs by CNQX/AP5 after 10 min confirms their feedforward nature. Right, representative current-clamp responses recorded before and after application of CNQX/AP5 in a representative deep (red) and superficial (green) CA1 PC. (**d**) The onset time of the evoked EPSC (at -70 mV) and IPSC (at +10 mV) was examined in the two cell types to evaluate potential differences. Right, no group differences were detected in the onset time of evoked synaptic currents. In both groups evoked IPSC lagged ESPC responses (EPSCs: $p<0.0001$, $t(11)=-7.19$; IPSCs: $p=0.0082$, $t(7)-3.64$; paired t-test). Note however slightly delayed EPSC onset in deep (red) versus superficial (green) cells. (**e**) Mean EPSC and IPSC recorded from deep and superficial cells at -50 mV in response to CA2 stimulation. No significant differences were detected at this holding potential, possibly reflecting current contamination. See **Fig.5l** for statistical differences between groups for EPSCs recorded at -70 mV and IPSCs recorded at +10 mV. (**f**) Upper plot: Relationship between the CA2-evoked EPSC amplitude (at -70 mV) and the distance to radiatum confirms stronger inhibition of CA1 deep cells. Bottom plot: Relationship between the CA2-evoked IPSC amplitude (at +10 mV) and the distance to radiatum confirms stronger excitation of CA1 deep cells.

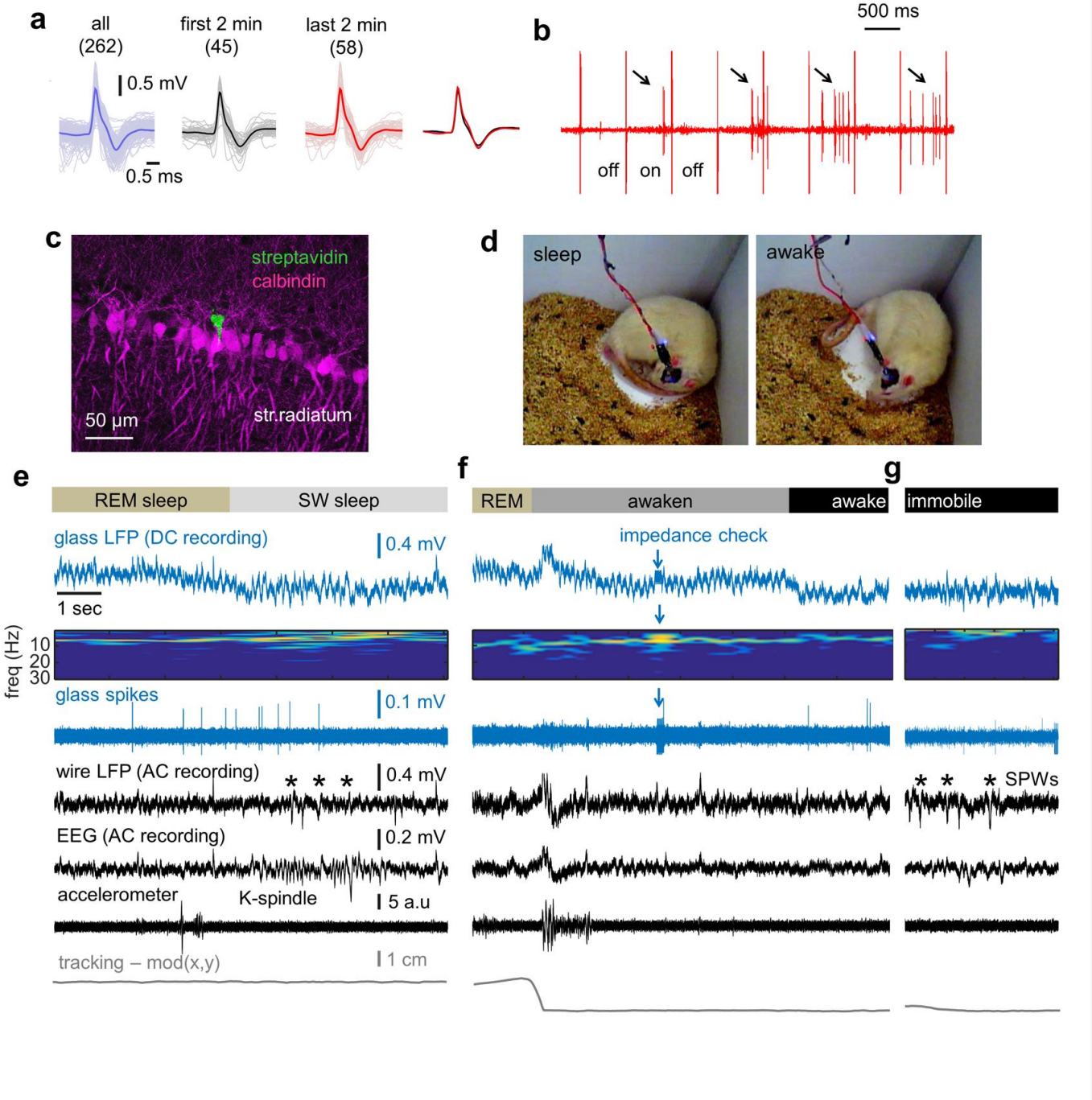

Supplementary Figure 7

Single-cell recordings in drug-free freely moving conditions and definition of behavioral states.

(**a**) Single-cells were recorded with glass pipettes in freely moving conditions. Spike waveform stability of cells with less than 1 ms peak-to-peak duration over at least 3 min recording session was used as inclusion criterion. The figure shows the example of a representative cell (rat75t1h1, 12.48 sec recording duration). All spikes from the whole session (blue) are compared with spikes recorded in the first 2 minutes (black) and in the last 2 minutes (red) before juxtacellular electroporation of Neurobiotin. The mean spike waveforms from all groups are shown together in the rightmost panel. (**b**) Same cell as before during juxtacellular electroporation (550 ms on-off pulses; 5-18 nA). Note firing modulation of the cell by positive pulses (on pulses), indicative of potentially successful electroporation. (**c**) Image of the cell shown before identified as a deep calbindin-immunonegative CA1 PC. 5 optical sections, 8.65 µm

thick. (**d**) Definition of behavioral states started by identifying awake and sleep epochs in the videos. Rats used to lay in a preferred corner. Sleep is characterized by a curled-up posture with eyes closed (left). Awake states were defined whenever the animals had their eyes open either moving or not (right). (**e**) Definition of behavioral brain states was subsequently refined using electrophysiological information from the glass pipette (LFP signals and their spectral features; blue) and the tracking position (gray bottom trace; modulus of the x,y vector). Glass pipette signals were acquired in direct-current (DC) mode. In two rats, we validated our approaches by using an additional wire LFP recording at the contralateral hippocampus (wire LFP) and an EEG screw at the prefrontal cortex acquired in alternating-current (AC) mode together with an accelerometer to account for tiny head movements. Rapid eye movement (REM) sleep was characterized by rhythmic activity at the theta band in the hippocampal LFP (4-12 Hz) accompanying small phasic movements of the head. The cortical EEG confirmed an association with low amplitude activity. Twitches were recorded by the accelerometer as small amplitude signals. Slow-wave (SW) sleep was characterized in the glass LFP signals by slow-wave activity during immobile curled-up postures. The cortical EEG showed occasionally k-complexes with spindles (k-spindle). Single-cell firing could be monitored during transition between states, as shown in this example. Note a DC-shift in the glass LFP associated to the REM-SW sleep transition. Sleep sharp-wave-ripples were identified (asterisks). Sleep recordings from the rat shown in **d** (left) (**f**) Awake states were defined whenever the animals open their eyes. In this example (same experiment as before) the animal awoke from REM sleep, moved the head, as detected both by the tracking and accelerometer signal and remained immobile. The hippocampal EEG showed a transition from theta activity to large irregular activity (note a DC-shift) while the cortical EEG remained low amplitude. Awake sharp-wave ripples were identified (asterisks). Glass pipette impedance was checked over the course of experiments to monitor indicative changes.

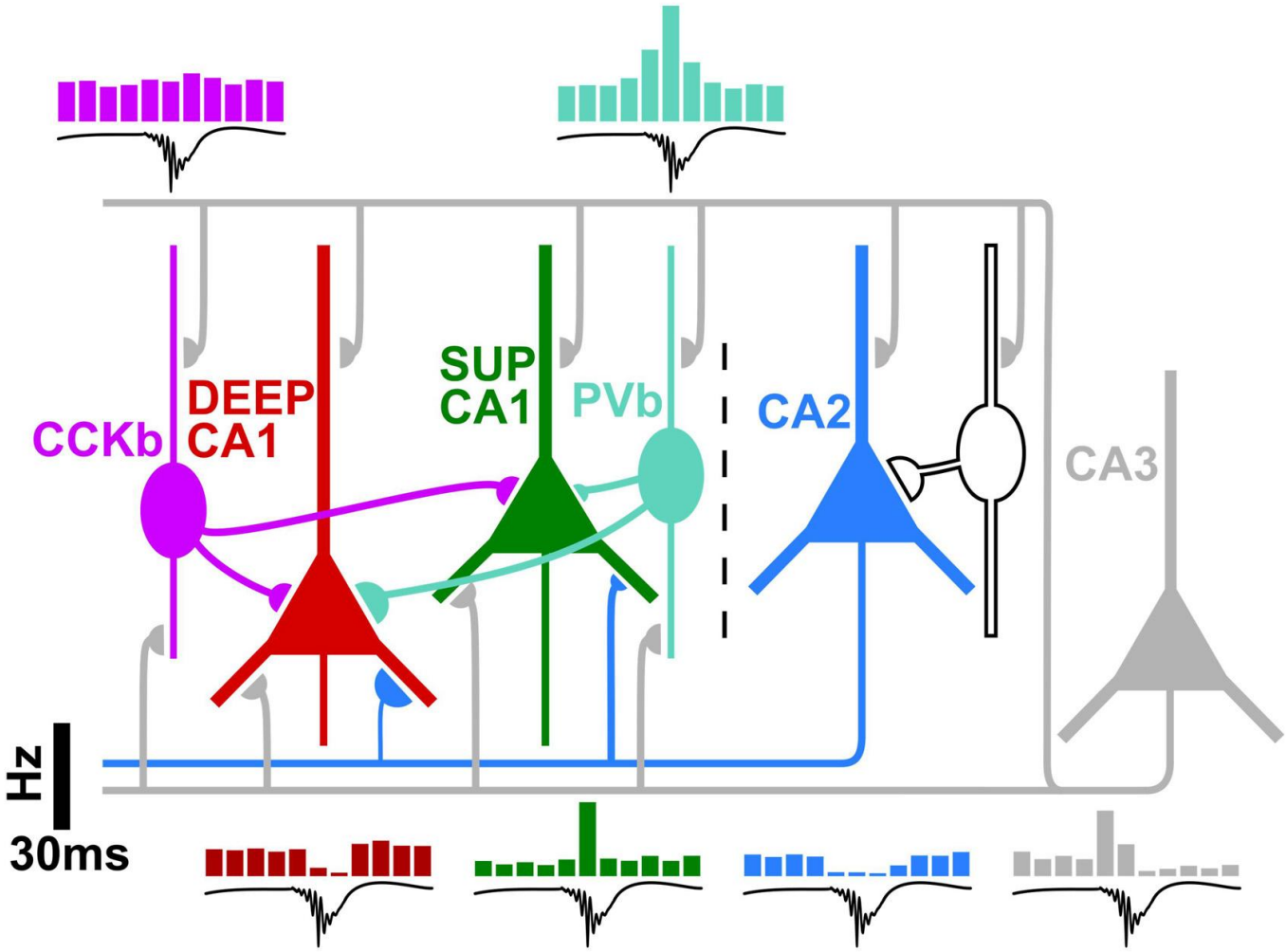

Supplementary Figure 8

Microcircuit mechanisms controlling heterogeneous CA1 behavior during SPW-ripple events

Schematic representation of the microcircuit mechanisms proposed to control heterogeneous CA1 behavior during SPW-ripple events. Firing from CA3 pyramidal cells (gray) propagate to activate downstream CA2 and CA1 pyramidal cells and local GABAergic interneurons. Schematic histograms reflect the major firing dynamics of each cell type. Firing from CA2 pyramidal cells (blue) is strongly suppressed by local feedforward inhibition (represented white) and release deep CA1 cells. As a result, PV-basket cells (PVb, cyan) which fire consistently during SPW-ripples and preferentially innervate deep CA1 sublayers, dominate the responses of deep CA1 pyramidal cells (red). Excitatory action dominates behavior of superficial CA1 cells (green), which are more likely to be innervated by CCK basket cells (CCKb, purple), which fire erratically during SPW-ripples.

Supplementary Table 1. Electrophysiological and morphological characteristics of CA1 pyramidal cells recorded in vivo

SPW: Sharp-waves; SPW-ass resp: SPW-associated response; depo: depolarized; hyper: hyperpolarized; SPW-r: SPW-ripple; RMP: resting membrane potential; AP amp: action potential amplitude; SP: stratum pyramidale; SR: stratum radiatum; CB: calbindin; Norm: normalized; sup: superficial;

Cell code	SPW-ass resp	RMP (mV)	AP amp (mV)	Input resistance (mΩ)	Recording duration (min)	SPW-ass peak resp (mV)	Nº SPW-r events (all)	Nº SPW-r events (sub-thr)	ML coord (mm)	AP coord (mm)	Dist to CA2 (mm)	Dist to SP/SR (µm)	Dist to probe track (µm)	Norm CB intensity	CB+/- class	sup/ deep class
I290212C5	depo.	-67.69	41.57	19.53	9.31	3.55 ± 2.7	10	5								
I050514D6C1	depo.	-58.78	66.92	14.46	22.243	0.78 ± 0.63	22	5	2.37	-3.30	0.39	8.91	394	0.46	+	sup
I130214B13C2	depo.	-63.15	43.12	40.90	30.98	4.84 ± 1.66	42	37	2.63	-4.30	2.00	22.99	183	0.18	-	sup
I130913B14C3	depo.	-63.43	59.72	20.01	66.70	6.86 ± 2.74	60	46	3.03	-3.40	1.51	17.86	483	0.37	+	sup
I130913B14C2	depo.	-64.74	58.84	24.99	27.13	3.69 ± 2.96	62	55	3.01	-3.60	1.44	49.89	499	0.29	+	deep
I080114A23C1	depo.	-54.26	55.40	11.84	29.367	1.05 ± 1.17	36	25	2.19	-4.16	1.59	4.57	220	0.41	+	sup
I060913C18C1	depo.	-61.48	55.00	19.68	20.13	4.61 ± 2.23	22	16	3.09	-3.80	1.03	34.54	610	0.13	-	sup
I021213B24C3	depo.	-64.0	59.83	12.79	20.56	6.96 ± 3.34	22	18	2.35	-3.60	0.61	42.12	237	0.50	+	sup
I030414D8C2	depo.	-58.48	46.23	25.30	11.41	2.23 ± 0.00	20	14	3.20	-4.80	1.75	14.86	1320	1.00	+	sup
I170614S88C2	depo.	-70.78	47.33	46.98	38.55	3.47 ± 2.45	37	30	3.20	-4.20	1.77	28.26		0.09	-	sup
I010714S54C3	depo.	-68.74	56.93	38.27	31.96	7.96 ± 2.36	14	10	3.20	-4.36	2.10	24.99		0.37	+	sup
I040913C2	depo.	-70.61	42.28	23.74	34.48	2.63 ± 2.16	43	39	2.90	-3.80	2.00	9.491	642	0.73	+	sup
mean ± SD		**-63.8 ± 5.1**	**52.8 ± 8.3**	**24.9 ± 11.4**	**28.6 ± 14.9**	**4.1 ± 2.3**	**32 ± 17**	**25 ± 16**	**2.84 ± 0.40**	**-3.94 ± 0.46**	**1.47 ± 0.57**	**23.50 ± 14.37**	**510 ± 347**	**0.41 ± 0.26**	**8/3**	**10/1**
I031012C1	hyper.	-60.14	45.39	21.08	32.91	-3.28 ± 3.01	112	100								
I290212C6	hyper.	-66.06	62.77	20.63	14.12	-2.94 ± 0.09	10	10								
I180713C5	hyper.	-61.50	52.79	20.70	26.47	-2.54 ± 4.15	25	18	2.70	-3.60	1.379	31.62	532	0.26	+	sup
I260314D5C1	hyper.	-59.6	51.39	16.26	24.99	-1.83 ± 2.08	74	54	2.64	-4.30	1.462	83.17	558	0.01	-	deep
I281112C2	hyper.	-60.43	44.77	25.01	32.66	-2.07 ± 2.70	58	58								
I230114B14C4	hyper.	-60.01	48.77	19.85	15.82	-3.36 ± 4.60	17	17	26.4	-4.16	1.87	32.66	366	0.15	-	deep
I130913B13C1	hyper.	-55.45	50.64	26.64	5.76	-0.44 ± 1.49	16	16	3.02	-3.60	1.43	54.74		0.19	-	deep
I100913D5C4	hyper.	-60.56	49.87	8.099	15.15	-4.33 ± 2.67	8	8	2.48	-3.80	1.49	55.13	143	0.05	-	deep
I101013B20C4	hyper.	-60.27	45.48	37.14	18.77	-2.67 ± 3.36	37	37	2.41	-3.80	2.41	23.07	486	0.17	-	sup
I061114C1	hyper.	-64.07	43.75	34.16	38.93	-0.51 ± 1.44	6	5	3.50	-3.72	0.4748	39.40		0.87	+	deep
mean ± SD		**-61.4 ± 2.9**	**49.6± 5.6**	**22.9 ± 8.4**	**22.6 ± 10.3**	**-2.4 ± 1.2**	**36 ± 35**	**32 ± 30**	**2.80 ± 3.75**	**-3.85 ± 0.27**	**1.50 ± 0.58**	**45.68 ± 20.39**	**417 ± 170**	**0.24 ± 0.29**	**2/5**	**2/5**
p-value (t test or x^{2}*)		0.176	0.313	0.663	0.295	**<0.001**	0.742	0.492	0.73	0.67	0.92	**0.015**	0.295	0.224	**0.066**	**0.006**

Supplementary Table 2. Electrophysiological and morphological characteristics of CA1 pyramidal cells recorded and labeled in drug-free conditions.

Spike amp: spike amplitude; Spike dur.: spike duration; Spike Asym index: spike asymmetry index; Autoc mode: autocorrelogram mode; SPW-r: sharp-wave-ripples; SPW-r part.: sharp-wave-ripple participation; Spatial test p-value: refers to the Fisher-Pitman permutation test for the firing rate during SPW-ripples; SP: stratum pyramidale; SR: stratum radiatum; CB: calbindin; Norm: normalized; sup: superficial.

Cell code	Spike amp (mV)	Spike dur. (ms)	Spike Asym index	Autoc mode (ms)	Firing rate awake (Hz)	Firing rate sleep (Hz)	Recording duration (min)	Nº awake SPW-r	Awake SPW-r part.	Nº sleep SPW-r	Sleep SPW-r part.	Open field (cmxcm)	Visited location (4x4)	Spatial test p-value	ML coord (mm)	AP coord (mm)	Dist to SP/ SR (µm)	Norm CB intensity	CB+/- class	Sup/ deep class
rat50t3h1	1.38	0.67	-0.36	6.0	1.48		3.12	64	0			40x40	1		2.44	-4.1	58.28			deep
rat75t1h1	1.35	0.62	-0.45	4.0	0.38	0.37	12.48	36	0.25	28	0.17	40x40	2	0.8119	1.85	-3.2	34.35	0.03	-	deep
rat83d1t1h3	1.32	0.59	-0.52	4.0	0.30	0.41	14.94	60	0.11	221	0.08	40x40	5	0.3665						
rat116t1h3	0.61	0.58	-0.28	5.0	1.63	0.16	13.74	155	0.27	25	0.16	40x40	4	0.8119						
rat123t1h1	1.64	0.71	-0.44	4.5	0.20	0.32	10.11	23	0.15	41	0.07	40x40	9	0.0494						
rat124t1h1	1.04	0.61	-0.36	4.5	0.23	0.22	14.55	48	0.02	140	0.04	40x40	3							
rat127t2h1	0.79	0.60	-0.57	4.0	2.63		43.70	100	0			40x40	1		2.38	-3.8	50.72	0.03	-	deep
rat138t2h2	1.90	0.85	-0.65	5.0	0.41		7.71	25	0.28			40x40	8	0.2574	2.47	-4.0	17.86			sup
rat147t1h1	0.75	0.70	-0.47	4.0	2.45		23.82	349	0.07			40x40	12	<0.0001	2.49	-3.5	28.35	0.13	-	deep
yfm2t2h4	1.7	0.95	-0.91	5.0	1.19		6.26	49	0.36			25x25	1		3.7	-3.0	23.78	0.70	+	sup
yfm6t1h4	1.83	0.67	-0.13	4.0	1.40	0.68	4.48	35	0.17	86	0.14	25x25	4							
Mean ± SD	**1.30 ± 0.45**	**0.69 ± 0.12**	**-0.46± 0.20**	**4.54 ± 0.65**	**1.11 ± 0.89**	**0.36 ± 0.18**	**14.08 ± 11.42**	**86 ± 95**	**0.15 ± 0.13**	**98 ± 78**	**0.11 ± 0.05**				**2.55 ± 0.61**	**-3.6 ± 0.44**	**35.43± 17.68**	**0.22± 0.32**		